Biomedical Research 2022; 33 (8): 247-255

ISSN 0970-938X
www.biomedres.info

Mirror-polished surface of ceria-stabilized zirconia/alumina nanocomposite enhancement in the adhesion strength of human gingival fibroblasts.

Takahito Osawa, Eri Urano-Morisawa, Fuminori Iwasa, Kazuyoshi Baba*

Department of Prosthodontics, School of Dentistry, Showa University, Kitasenzoku, Oota-ku, Tokyo 145-8515, Japan

Abstract

Connective tissue sealing between the transmucosal area of the dental implant surface and the soft tissue is important for the long-term stability of dental implants. This study aimed to investigate the mechanical adhesion strength of the Connective Tissue Equivalents (CTEs) to the Ceria-stabilized Tetragonal Zirconia Polycrystal/Alumina (Ce-TZP/Al_2O_3) surface. We prepared Titanium (Ti) and Ce-TZP/Al_2O_3 disks with different surface roughness, namely, mirrored and machined surfaces, on which HGF-1 were cultured, and then the biological parameters of the cultured cells, including cell morphology and gene expression of focal adhesion proteins were assessed. Furthermore, the mechanical adhesion strength of CTEs to the disk surface was measured using the nano-scratch test. Scanning electron microscopy and atomic force microscopy observation showed smoother morphology on the mirror-polished surface when compared to the mechanically polished surface. A lager expansion of the cell area accompanied by a greater development of actin cytoskeleton and talin1, a greater adhesion strength of CTEs to each disk, and higher gene expression level of focal adhesion protein were observed with the mirror-polished surface than the mechanically polished surface both Ti and Ce-TZP/Al_2O_3 disks. No such differences were found between Ti and Ce-TZP/Al_2O_3 disks. This study provides the first evidence for the mechanical adhesion strength of CTEs to Ce-TZP/Al_2O_3 and Ti surfaces. Mirror-polished Ce-TZP/Al_2O_3 might contribute to the success of implant therapy by its strong adhesion strength to gingival connective tissues with the developed focal contact-cytoskeleton complex.

Keywords: Connective tissue equivalents, Mechanical adhesion strength, Nano-scratch test.

Accepted on October 12, 2022

Introduction

Dental implants and implant-supported prostheses are common treatments for replacing missing teeth. Sufficient bone-implant integration is primarily required for a successful dental implant [1]. In this context, a significant number of studies aiming at improving the integration between the bone and surface of the dental implants were released [2]. In addition, to ease wound healing and soft tissue sealing, it is essential to have compatibility between the connective tissue and the implant neck region facing the gingiva [3]. If soft tissues do not attach quickly and firmly to the implant, bacterial infections can occur around the implant neck region, precisely in the connective tissue, which can lead to peri-implant diseases [4,5]. Consequently, it is crucial to improve the implant surface to increase its affinity with bone and connective tissues.

From another side, fibroblasts are important in connective tissues production, remodelling, and creating a peri-implant barrier [6]. Therefore, retaining the fibroblasts on the surface of a material is necessary to establish integration with soft tissue, and particularly for implant abutments sealing [7]. The resistance of cells on a biomaterial to compressive, tensile, or shear forces largely depends on the cell adhesion strength [8]. This is controlled during the cell adhesion procedure through molecules and signalling pathways following a biological cascade, including proliferation and Extracellular Matrix (ECM) production [9]. Throughout cell–material interaction, adhesion is influenced by the features of a biomaterial surface, comprising topography and physicochemical properties. In principle, cells tend to spread broader on a smooth and/or more hydrophilic surfaces [10,11].

In implants, Zirconium (Zr) abutments are potential substitutes to Titanium (Ti) and offer better aesthetic result [12]. Furthermore, Zr can replace metals in both clinical medicine and dentistry owing to its high level of mechanical strength and excellent bioactivity [13]. In 1998, improvements in nanotechnology developed a strong Ceria-stabilized Tetragonal Zirconia Polycrystal/Alumina (Ce-TZP/Al_2O_3) nanocomposite, which has an interpenetrated intragranular nanostructure. Within this structure, each nanometer-sized particles of Ce-TZP or

Al_2O_3 are found in submicron-sized grains [14]. The Al_2O_3 phase dispersed homogeneously increases the hardness, elasticity modulus, and hydrothermal stability. Moreover, compared with conventional 3Y-TZP, Ce-TZP/Al_2O_3 exhibits greater flexural strength and fracture hardiness, making it appropriate for dental implants use [15,16]. Our previous studies on animals confirmed the overcome of the osseointegration strength of Ce-TZP/Al_2O_3 treated with hydrofluoric acid on acid-etched Ti implants [17]. Furthermore, we proved the improvement of gingival fibroblast biological affinity on a totally smooth surface without roughness or topographic features, such as mirror-polished Ce-TZP/Al_2O_3 surfaces (MrZr), as supported by markedly expedited cell spread, dense actin fiber formation, and upregulated expression of collagen and fibronectin, which functions as a key scaffold protein in focal adhesion plaques and is involved in linkage of integrin adhesion molecules to the actin cytoskeleton [18].

An advanced focal contact–cytoskeleton complex and enhanced cell spread behavior propose that MrZr considerably promises fibroblastic retention [18]. An indirect indication of enhanced adhesion strength of fibroblast on materials surfaces can be simply shown by morphologic cell observation. Nevertheless, a quantitative comprehension of cell adhesion is needed to elucidate the biological mechanism underlying the bio-activation of Ce-TZP/Al_2O_3 and intracellular behavior between cells and MrZr. Thus, measuring direct indicators of retention such as the critical force required to scratch the tissues on MrZr is important. For this purpose, we established a shear test device to assess cells and their ECM detachment force. This device shows the direct values of the critical force required to detach a tissue, that is, cell and ECM, from a material surface.

This study aims to measure and compare the retention capacity of fibroblasts and ECM on MrZr in terms of critical load values between the machined surfaces of Ce-TZP/Al_2O_3 (MZr) and Ti (MTi) with similar surface roughness using the nano-scratch test and compute the degree of cell spread, cytoskeletal development, and focal adhesion assembly.

Materials and Methods

Sample preparation

We mechanically prepared disks (diameter 20 mm × thicknesss 1.0 mm; #325) of commercially pure grade 4 MTi (Nishimura, Fukui, Japan) and MZr (Yamakin, Osaka, Japan) by means of a forming surface grinder (NSG515AD2; Nicco, Kyoto, Japan). To standardize the roughness of MTi surfaces, we polished MZr for each disk using waterproof abrasive paper (#600). We prepared MrTi and MrZr by buffing with 0.01 μm of diamond paste after polishing using waterproof abrasive paper (#600 and #1200). To prevent contamination, we stockpiled these disks one by one at room temperature; then, we cleaned them with acetone and washed them *via* ultrasonication in a series of ethyl alcohol and distilled water for 10 min. Next, we autoclaved the disks at 121°C under 0.20 MPa (TOMY SX-500, High-Pressure Steam Sterilizer). Afterward, we used them instantly in the culture experiments after being arranged on 12-well culture-grade polystyrene plates.

Surface analysis

After polishing each disk, we calculated the average of the surface roughness (Ra) with a surface profile meter (Surfcom 480A; Tokyo Seimitsu, Tokyo, Japan) at five different points. We observed the surface morphology through a Scanning Electron Microscope (SEM) (Miniscope TM3000; Hitachi High-Technologies, Tokyo, Japan) and an Atomic Force Microscope (AFM) (PS-NEX; Research Institute of Biomolecule Metrology, Ibaraki, Japan). From another side, we determined the disks wettability as the Contact Angle (CA) using a CA meter (SImage Mini, Excimer, Yokohama, Japan). Using an attached injector, we dropped 5 μl of distilled water onto the center of the specimen. Using goniometry software, we evaluated and represented CA's from the captured images as average values with their standard deviations. For each specimen, we repeated the measurements three times.

Cell culture

HGF-1 obtained from American Type Culture Collection (Manassas, VA, USA) was cultured in Dulbecco's modified Eagle's medium, supplemented with 10% fetal bovine serum (PAA Laboratories, Manassas, VA, USA) and 1 mmol/L L-ascorbic acid 2-phosphate (Asc-2P; Wako Pure Chemical Industries Ltd, Osaka, Japan). Antibiotics Antimicrobial Solution (Nacalai tesque, Kyoto, Japan) were incubated in a humidified atmosphere at 37°C (95% air; 5% CO2). When 80% of confluency was roughly reached, we separated and seeded the cells with 0.05% trypsin in 1 mmol/L Ethylenediaminetetraacetic acid tetrasodium salt (EDTA-Na4) onto disks in 12-well plates at a density of 2.5×10^4 cells/cm^2. We changed the medium every 3 days and conducted the cultures for 1 week (7 days). In this study, we used the cells from passages 3-8. As fibroblasts accumulate collagen and ECM when Asc-2P is added, resulting in three-dimensional structures [19], we named this product CTEs (Connective Tissue Equivalents) in this study as well.

Cell morphology

We performed immunohistochemical staining with talin1 (CellLight™ talin-Green Fluorescent Protein (GFP) BacMam 2.0) and actin (CellLight™ actin-Red Fluorescent Protein (RFP), BacMam 2.0; Thermo Fisher, USA). We stored the samples at 4°C and cultured and observed the morphology and cytoskeletal organization of HGF-1 on various Ce-TZP/Al_2O_3 and Ti surfaces under a fluorescence phase contrast microscope (BZ-X710; Keyence, Osaka, Japan). We measured the cell area in the confocal images using an image analyzer (BZ-X Analyzer; Keyence, Osaka, Japan).

Real-time Reverse Transcription quantitative PCR (RT-qPCR)

Many structures that link extracellular and cytoskeletal elements, among which are talin1, vinculin, and paxillin, are considered as major proteins involved in cellular adhesion, thus playing a key role in the focal adhesion process [20]. Therefore, we investigated the distribution of these proteins under different experimental conditions. Following the manufacturers' protocols, we extracted and reverse-transcribed total RNA from cultured cells using ISOGEN® (Nippon Gene Co., LTD., Tokyo, Japan) and Super Script III First-Strand Synthesis System® (Thermo Fisher) through a Veriti® 96-Well Fast Thermal Cycler (Applied Biosystems). We performed RT-qPCR with PowerUp SYBR™ Green Master Mix (Applied Biosystems) using a QuantStudio 3® (Applied Biosystems), under the following conditions: activation of Uracil-DNA glycosylases: 2 min at 50°C; activation of Dual-Lock™ DNA polymerase: 10 min at 95°C; and dissociation of the melting curve: 40 cycles for 15 s at 95°C, 1 min at 60°C, 15 s at 95°C, 1 min at 60°C, and 1 s at 95°C. We used specific forward and reverse oligonucleotide primers in conjunction with Power Up SYBR Green® dye (Thermo Fisher) (Table 1). The level of mRNA expression was normalized to that of glyceraldehyde 3-phosphate dehydrogenase mRNA.

Nano-scratch test

We performed the whole experiment using a Triboindenter system (Hysitron Inc. TI950, Minneapolis, MN, USA) under constant environmental conditions (24°C, 35% H) (Figure 1). To detect the force of adhesion of the connective tissue by CTE on disks, we used the nano-scratch test. We carried out the calibration process using the Triboindenter system on a fused quartz standard specimen. To determine the scratch sites, we identified CTE on the disks *via* optical microscopy (Figure 2A, a). Then, to confirm that scratching had been performed, we checked the *in situ* Scanning Probe Microscopy (SPM) imaging before (Figure 2B, b) and after (Figure 2D, d) scratching. From the first contact of the cell probe (Figure 2C, c-x), the coefficient of friction increases with a rise in lateral force (Figure 2C, c-y), and the maximum coefficient of friction (point y) leads to the initiation of the first cell detachment (Figure 2C). In this study, we defined point y as the critical load value by virtue of recording a steady data compared to those after the first detachment (Figure 2C, c-z). In a nano-scratch test, the coefficient of friction is computed by dividing the lateral force to the normal force [21,22]. As a probe, we used a conical diamond indenter tip with a diameter of 0.5 μm, which is less sensitive to the direction of scratching. We performed the nano-scratch test under the normal load of 1,000 μN, with a scratch length of 10 μm and a constant scratching speed of 0.5 μm/s. For each sample, we repeated the test four times and computed the average value as the measured value of the disk.

Table 1. *Primers used for qPCR.*

Gene	Forward primer sequence (5'-3')	Reverse primer sequence (3'-5')
GAPDH	GAATCCACCGGTGTCCTCAC	TCCTTCCACGATACCGGAGT
Talin1	CGTGCAAACCAGGCAATTCA	CTCTTGGACTGCAGTGAGCA
Paxillin	GATCCCTAACCGGGCCTTAG	TGATGGGTCCTTGAAACGGG
Vinculin	CGCCGAGGGTTCGAATGG	GAAAAACCGGGCTTGTGGTC

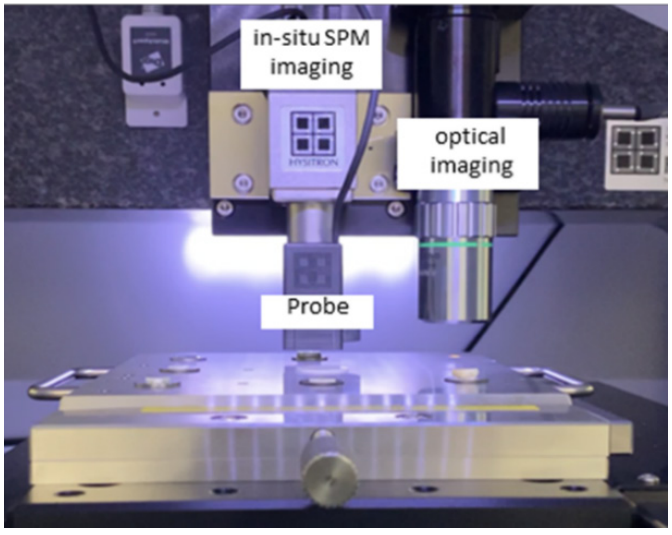

Figure 1. *Picture of the inside of a Triboindenter. Optical microscopy,* in situ *SPM imaging, and nano-scratch tests were performed in the same site under mechanically controlled conditions in the Triboindenter.*

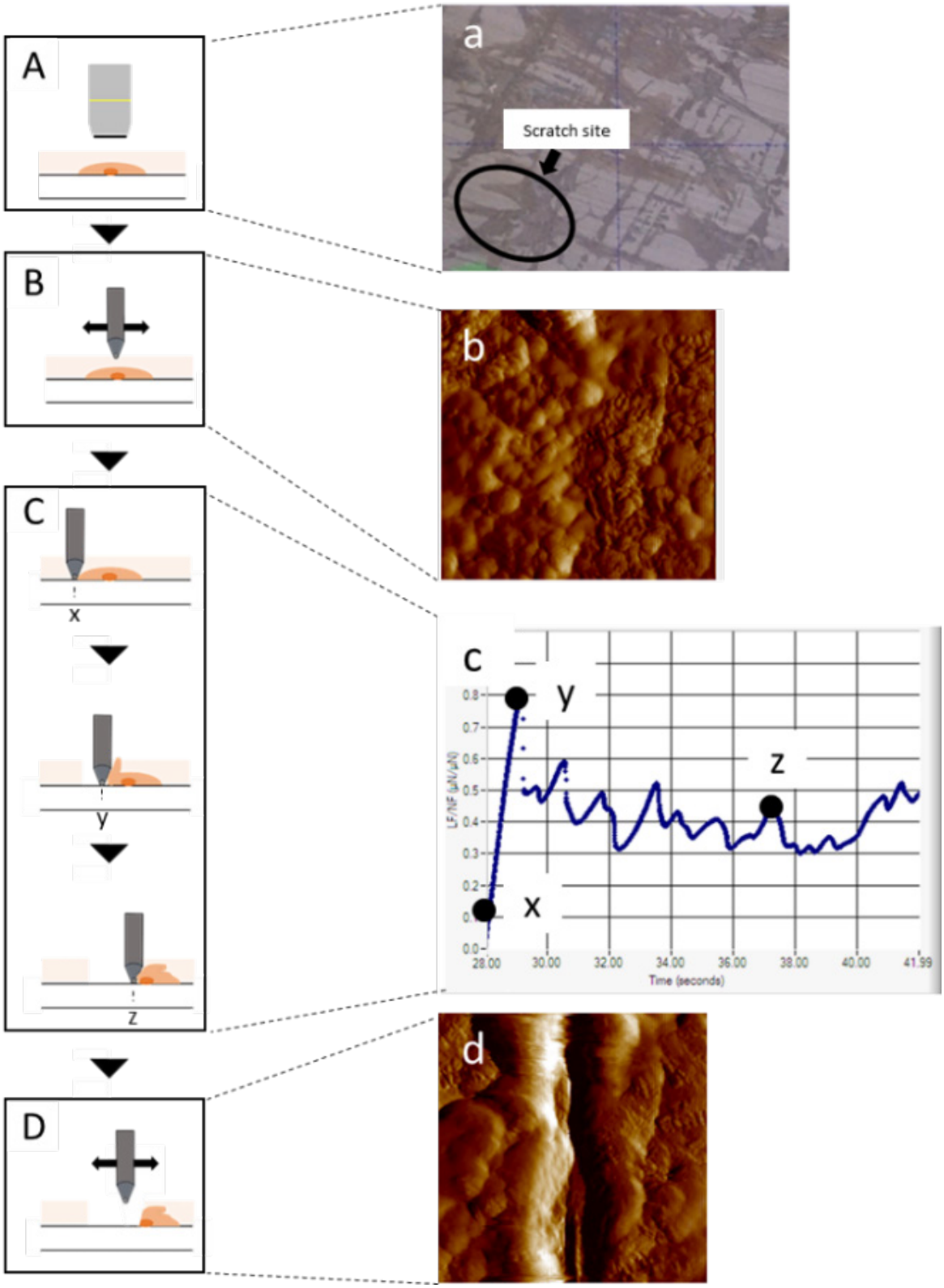

Figure 2. *The sequences and methods of nano-scratch test. A: The screen (a) determining the site of measurement in the sample by optical microscopy. B, D: Representative figures in SPM images: (b) before and (d) after scratching. Scratching direction is from bottom to top. (d) The middle area with a change in morphology is the trace of probe passing through. C: Representative curves of friction coefficients (c) obtained from the scratch test. Point x is where the tip of the cantilever first contacts the single cell, whereas point y is assumed to be the point where the magnitude of the pushing force reaches its peak and cell detachment is initiated. The pressing force turned to decrease, and detachment continued within the range of probe movement (point z). The maximum force at point y was defined as the critical load value.*

Statistical analysis

To evaluate the effect of the substrate on cell spread, protein synthesis, and critical load values, we applied two-way analysis of variance. For multiple comparisons, we performed the Tukey test. Significance was considered for $P<0.05$.

Results

Surface morphology

The Ra values of MTi and MZr were 0.98 and 0.93 μm, respectively. Also, the Ra values of MrTi and MrZr were 0.02 μm. Noting these, all sample surfaces of Ti and Zr disks were hydrophilic (CA of $H_2O<50°$). Owing to polishing treatment, the changes in CA of Ti and Ce-TZP/Al_2O_3 surfaces were reduced from 43.5° to 35.3° and 30.1° to 25.1°, respectively. Therefore, MrZr surfaces presented the lowest CA among all the surface properties (Table 2). SEM and AFM profiles revealed that the surface morphologies of both MTi and MZr disks were relatively smooth and flat, with some typical residual traces left from the grinding process (Figures 3A and 3B). In contrast, the SEM images of MrTi and MrZr disks showed very smooth and flat morphologies, without topographical or rough features (Figures 3C and 3D).

Table 2. *Surface roughness and contact angle.*

	MTi	MrTi	MZr	MrZr
Ra (μm)	0.92 ± 0.06	0.02 ± 0.03	0.91 ± 0.04	0.02 ± 0.02
CA	43.5° ± 1.3	35.3° ± 1.4	30.1° ± 1.1	25.1° ± 1.3

Cell morphology and spreading on Ce-TZP/Al2O$_3$

At 1-week cultivation, after actin staining with RFP, the fluorescence phase contrast microscopy images of HGF-1 revealed that HGF-1 deposition on the MrZr surface overcame MZr. In addition, the cells on mirrored surfaces consistently showed significantly higher values than those on machined surfaces for the following cytomorphometric parameters: cell area, perimeter, and diameter. The shapes of HGF-1 on both machined surfaces have several common characteristics including spindle-shaped and small protrusions (Figures 4A and 4C). In contrast, HGF-1 deposits on both mirrored surfaces were widely spread with large protrusions (white arrows in Figures 4B and 4D). Fluorescence phase contrast microscopy images, after anti-talin1 staining (Figures 4A-4D), labeled with GFP, and overlaid with images of actin expression, showed that fibroblasts on both surfaces expressed talin1 in their cytoplasm and at the tip of their extended cellular projections at 1-week incubation.

mRNA expression of adhesive protein

The gene expression of focal adhesion proteins represents both the development of focal adhesion and the activation of subsequent signal transduction. First, the gene expression of talin1 upregulated equally the result of confocal image, so it reflects the widespread of cell. Expression of talin1 and vinculin in an individual fibroblast was substantially about 1.5 times significantly higher on MrZr than on MZr at 7-day incubation (Figure 5A). Similarly, the identified expression on MrTi was around 1.4 times significantly higher than that on MTi (Figures 5B and 5C). In contrast, paxillin expression levels were not significantly different between MZr and MrZr. However, the extent of talin1, paxillin, and vinculin expression divided by the cell area on both mirrored and machined surfaces was proportionally the same (data not shown).

Nano-scratch test

The critical load values of CTE on Ti and Ce-TZP/Al_2O_3 were measured using the nano-scratch test. At 7-day incubation, the mean value required to initiate detachment of CTE on MrZr was 1.3 times significantly greater than that on MZr (0.83 ± 3 μN to 0.64 ± 4 μN, respectively) (Figure 6). Similarly, the force level on MrTi remained almost the same as Ce-TZP/Al_2O_3 even at 7-day incubation (0.78 ± 4 μN), yet it was significantly greater than that on MTi (0.61 ± 1 μN). The force on MrZr tended to be insignificantly higher than that on MrTi ($P<0.05$).

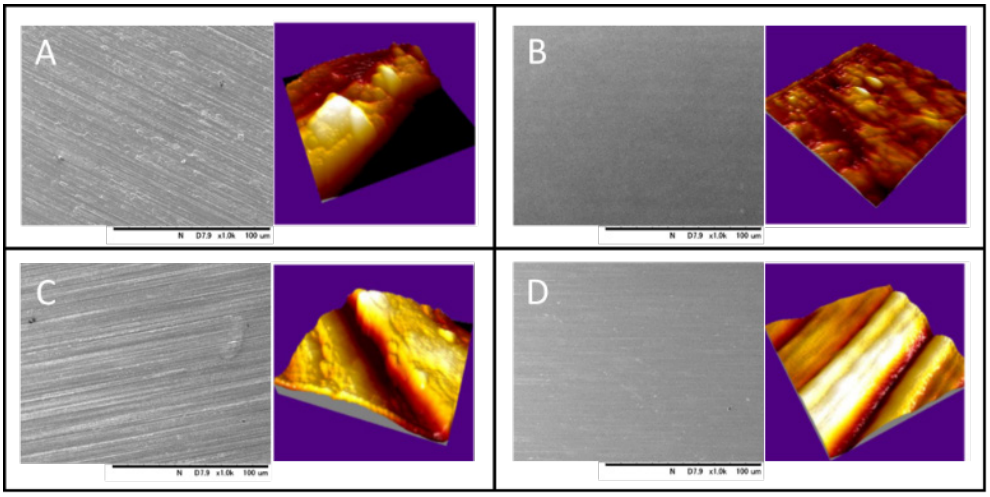

Figure 3. *Different surface roughness profiles of Ti and Ce-TZP/Al2O3 disks characterized by SEM and AFM. The SEM images at 1,000 × magnification (A: MTi, B: MrTi, C: MZr, D: MrZr). The figure on the right is taken by SEM and the one on the left by AFM.*

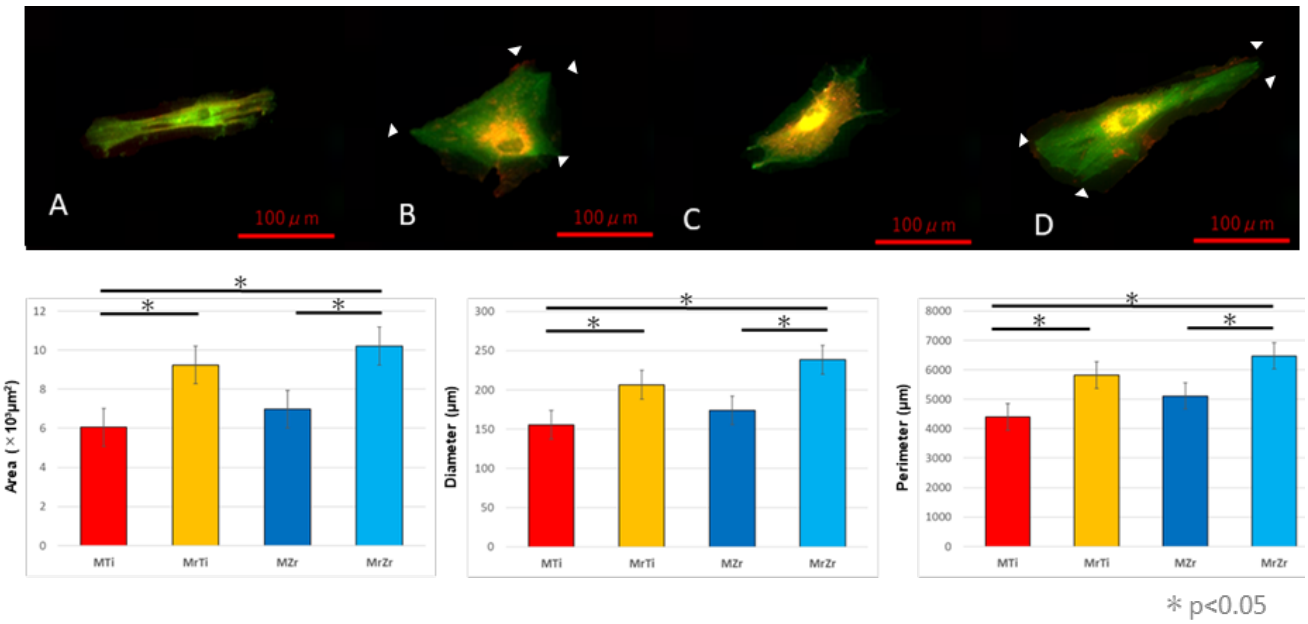

Figure 4. *Fluorescence phase contrast microscopy images (A: MTi, B: MrTi, C: MZr, D: MrZr) of the spreading, cytoskeletal composition, and talin1 distribution of HGF-1 cultured on Ti and Ce-TZP/Al2O3 for 7 days. Talin1 expression concentrated at the tip of cellular projections was seen only on mirrored surfaces (white arrow in B and D). Cell area, diameter, and perimeter were measured and evaluated using an image analyzer (BZ-X Analyzer; Keyence, Osaka, Japan). Data are presented as mean ± standard deviation (n=10). *P<0.05, showing statistically significant differences between several experimental groups.*

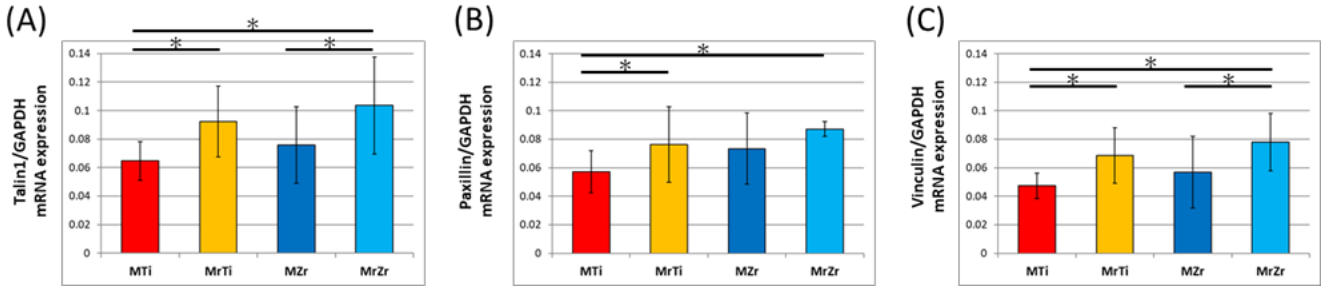

Figure 5. *Expression levels of mRNA for talin1 (A), vinculin (B), and paxillin (C) in HGF-1 cultured on each disk for 7 days. qPCR was performed more than five times in triplicate. *P<0.05.*

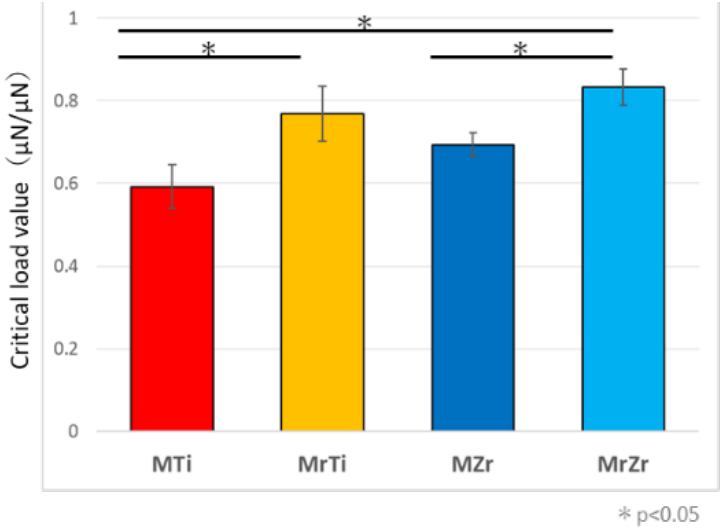

Figure 6. *The average critical load values of the four test substrates with standard deviations (n=5). *P<0.05, indicating a statistically significant difference between multiple experimental groups.*

Discussion

First, we evaluated the quality of the polished Zr and Ti disks using a surface profile meter. The detected Ra values of Ce-TZP/Al_2O_3 and Ti surfaces were approximately 0.022 and 0.023 μm, respectively, which were lower than that of the culture-grade polystyrene plate (approximately 0.05 μm) [23]. Therefore, the mirror-polished surfaces used in this study could be considered as extremely smooth, with no significant topographical structures excluding their unique linear grooves.

Cell adhesion reinforcement would lead to the avoidance of cell detachment by external forces [24]. In addition, for anchorage-dependent cells such as fibroblasts, the enhancement of attachment behavior influences their subsequent function on a scaffold [25]. Fluorescence microscopic images showed that cell adhesion was stimulated and improved on mirror-polished surfaces compared to that on roughened surfaces. In this context, fibroblasts exhibited a well-elongated shape with development of cellular projections and a compact cytoskeletal structure (Figures 4B and 4D). Moreover, actin filaments were well arranged at 7-day incubation and appeared at a greater density and intensity than those on roughened surfaces (Figures 4A and 4C). These results, which are consistent with those of our earlier studies, show that mirrored surfaces accelerated and increased the cytoskeletal development of the fibroblasts.

The minimum load value at which delamination of the coating is detected is a critical characterization for the mechanical resistance of the interface. This technique is recognized in engineering to assess the adhesion properties of films and coatings [26]. In general, this measurement depends on inherent parameters (scratching speed, loading rate, diamond tip radius, diamond wear, etc.) and external parameters (coating thickness) [27,28]. In this study, we designed a measurement system by modifying the nano-scratch test, which is one of the interface delamination technologies, to assess the adhesion properties of the interface between tissues containing fibroblasts and test surfaces. In addition, we clearly detected the exfoliation points of tissue samples by handling *in situ* SPM images (Figures 2b and 2d). As a consequence, the relatively small standard deviations between the calculated critical load values indicate that the measurements are reproducible along with the adopted loading forces and velocities. Mirror polishing treatment modified adhesion strength and the cellular adhesive properties of individual fibroblasts. For example, the critical load values needed to detach CTE from Ti and Ce-TZP/Al_2O_3 were, respectively, 1.29 and 1.32 times higher on mirror-polish surfaces than on roughened surfaces at 7-day after culture. These results clearly indicate that cell retention is strongly increased on mirror-polished surfaces, resulting in greater resistance to shear and compressive force that might cause cell detachment even in the final stage of cell adhesion.

Complexes of focal adhesions are particular structures that organize a large number of cytoskeletal molecules and intracellular signalling proteins in cells [29]. These multimolecule complexes are important in aggregating and integrating many signals from both extracellular and intracellular environments [30]. Through the integrin family, such signals transmit cell membrane adhesion molecules to adapter proteins in the focal adhesion plaque, including talin1 and vinculin [31]. Furthermore, these adapter proteins have binding sites for actin filaments and signalling molecules, including paxillin and Focal Adhesion Kinase (FAK), which regulate the formation of cellular projections and the cytoskeletal actin fiber network [32]. In particular, paxillin emerged as a key coordinator of the Rho family of GTPases, which dominates the signaling process in relation to cell spreading. Moreover, vinculin is important in initiating and establishing cell adhesion, formation of cell shape, and cytoskeletal development, which is indispensable for the coordinated control of fundamental cellular processes, including differentiation, cell cycle control, apoptosis, and motility [33]. In a focal adhesion plaque, the amino-terminal in the vinculin molecule binds to talin1, which, in turn, binds to β-integrins, whereas the carboxy-terminal binds to actin, phospholipids, and paxillin-forming homodimers [34,35]. In addition to the recruitment of the cytoskeleton and vinculin, the number of bound integrin receptors and the focal adhesion combining those receptors are known to regulate cell adhesion strengthening [36]. The expedition and advancement of cell spread accompanying focal adhesion assembly and cytoskeletal development as identified above may contribute to the enhancement of the capability of fibroblasts to adhere to mirror-polished surfaces, which have unique characteristics such as hydrophilicity, extremely smooth with micro-grooves created during the polishing process.

Nevertheless, the region at which fibroblasts become completely detached was unclear in molecular levels, even though traces of individual cells were detected by SPM after delamination. There are several hypothetical detachment styles such as extracellular abruption at integrin-ECM bonds or at the ECM-material surface, and disruption of intracellular bonding between integrin-vinculin and vinculin-actin [32]. The detachment style is influenced by the following: type and quality of ECM, cell type, form and number of integrin ligands, and material's surface characteristics. However, the cell-material interactive mechanism underlying bio-activation on mirror-polished surfaces needs to be fully clarified. Protein absorption and synthesis, including those of collagen and fibronectin, markedly increases on surfaces after mirror polishing [18,37]. Based on the results of an earlier study, we assumed that hydrophilicity of the substrate might promote interaction with proteins and cells. However, the difference of hydrophilicity between mirrored and machined surfaces was not significantly observed (Table 2). Other physicochemical surface properties

such as electrical charge, elemental distribution, and molecular attraction would be needed for further research. Clarification of how interfacial signal transmission from material to cell results in fibroblastic affinity and adhesion strengthening on mirror-polished Zr and Ti surfaces would be of great interest.

In the dental field, Zr material is essential not only for bone anchorage but also for aesthetic devices, including dental crown and dental implant abutment [38,39]. Therefore, fibroblasts must adhere to Zr surfaces with polished topographies in the aesthetic region of dental devices. When taken together with the results of earlier studies on rough-surface Zr such as machined, acid-etched, and sandblasted, the obtained results using very smooth MrZr might contradict some widespread trends in cell retention property.

Conclusion

In conclusion, we enhanced the strength of the tissue adhesion that contains fibroblast and ECM equally on MrZr and MrTi with a very smooth mirror-polished surface, detected using the nano-scratch test. The reinforcement of the cellular retention capability was supplemented by a clear improvement of cell spread and cytoskeletal development and an increase in expression levels of talin1, vinculin, and paxillin. The results of this study also indicate the possible effectiveness of the mirror-polished surfaces for fibroblastic activation on any bulk material, regardless of the surface element, suggesting that MrZr may be able to acquire a stronger sealing to soft tissues.

Acknowledgment

The authors would like to thank Dr. Yo SHIBATA (Department of Conservative Dentistry, Division of Biomaterials and Engineering at Showa University) for general support of the study. We also thank all the members of our laboratory. This study was supported by a Japan Society for the Promotion of Science KAKENHI grant (grant no. 21K10009).

References

1. Shah FA, Thomsen P, Palmquist A. Osseointegration and current interpretations of the bone-implant interface. Acta Biomater 2019; 84: 1-15.
2. Pandey C, Rokaya D, Bhattarai BP. Contemporary concepts in osseointegration of dental implants: A review. Biomed Res Int 2022; 2022: 6170452.
3. Ikeda T, Ueno T, Saruta J, Hirota M, Park W, Ogawa T. Ultraviolet treatment of titanium to enhance adhesion and retention of oral mucosa connective tissue and fibroblasts. Int J Mol Sci 2021; 22: 12396.
4. Buser D, Sennerby L, de Bruyn, H. Modern implant dentistry based on osseointegration: 50 years of progress, current trends and open questions. Periodontol 2000 2017; 73: 7–21.
5. Atsuta I, Ayukawa Y, Kondo R, Oshiro W, Matsuura Y, Furuhashi A, Tsukiyama Y, Koyano K. Soft tissue sealing around dental implants based on histological interpretation. J Prosthodont Res 2016; 60: 3-11.
6. Smeets R, Henningsen A, Jung O, Heiland M, Hammächer C, Stein JM. Definition, etiology, prevention and treatment of peri-implantitis: A review. Head Face Med 2014; 10: 1-3.
7. Kensy J, Dobrzyński M, Wiench R, Grzech-Leśniak K, Matys J. Fibroblasts adhesion to laser-modified titanium surfaces: A systematic review. Materials 2021; 14: 7305.
8. Wang L, Wu S, Cao G, Fan Y, Dunne N, Li X. Biomechanical studies on biomaterial degradation and co-cultured cells: Mechanisms, potential applications, challenges and prospects. J Mater Chem B 2019; 7: 7439-7459.
9. Hu M, Ling Z, Ren X. Extracellular matrix dynamics: Tracking in biological systems and their implications. J Biol Eng 2022; 16: 1-3.
10. Beheshti Maal M, Aanerød Ellingsen S, Reseland JE, Verket A. Experimental implantoplasty outcomes correlate with fibroblast growth in vitro. BMC Oral Health 2020; 20: 1-11.
11. Areid N, Peltola A, Kangasniemi I, Ballo A, Närhi TO. Effect of ultraviolet light treatment on surface hydrophilicity and human gingival fibroblast response on nanostructured titanium surfaces. Clin Exp Dent Res 2018; 4: 78-85.
12. Fontana D, Ruppenthal S, May A, Aktas C, Mehraein Y, Lipp P, Kaestner L. Differential behavior of fibroblasts and epithelial cells on structured implant abutment materials: A comparison of materials and surface topographies. Clin Implant Dent Relat Res 2015; 17: 1237-1249.
13. Chopra D, Jayasree A, Guo T, Gulati K, Ivanovski S. Advancing dental implants: Bioactive and therapeutic modifications of zirconia. Bioact Mater 2022; 13: 161-178.
14. Ban S, Sato H, Suehiro Y, Nakanishi H, Nawa M. Biaxial flexure strength and low temperature degradation of Ce-TZP/Al_2O_3 nanocomposite and Y-TZP as dental restoratives. J Biomed Mater Res Part B Appl Biomater 2008; 87: 492-498.
15. Coutinho IF, Cipriano da Silva P, Moreira LP, Strecker K, Alves MFRP, Santos CD. Experimental analysis and numerical simulations of the mechanical properties of a (Ce,Y)-TZP/Al_2O_3/H6A ceramic composite containing coupled toughening mechanisms. J Mech Behav Biomed Mater. 2022; 129: 105171.
16. Santos CD, Coutinho IF, Amarante JEV, Alves MFRP, Coutinho MM, Moreira da Silva CR. Mechanical properties of ceramic composites based on ZrO2 co-stabilized by Y2O3-CeO2 reinforced with Al_2O_3 platelets for dental implants. J Mech Behav Biomed Mater. 2021; 116: 104372.
17. Oshima Y, Iwasa F, Tachi K, Baba K. Effect of nanofeatured topography on ceria-stabilized zirconia/alumina nanocomposite on osteogenesis and osseointegration. Int J Oral Maxillofac Implants 2017; 32: 81-91.
18. Akiyama Y, Iwasa F, Hotta Y, Matsumoto T, Oshima Y, Baba K. Effects of surface roughness of ceria-stabilized zirconia/alumina nanocomposite on the morphology and function of human gingival fibroblasts. Dent Mater J 2021; 40: 472-480.
19. Ishikawa O, Kondo A, Okada K, Miyachi Y, Furumura M. Morphological and biochemical analyses on fibroblasts and self-produced collagens in a novel three-dimensional culture. Br J Dermatol 1997; 136: 6-11.
20. Atherton P, Lausecker F, Carisey A, Gilmore A, Critchley D, Barsukov I, Ballestrem C. Relief of talin autoinhibition triggers a force-independent association with vinculin. J Cell Biol 2020; 219: e201903134.

21. Gao S, Gao S, Xu B, Yu H. Effects of different pH-values on the nano-mechanical surface properties of PEEK and CFR-PEEK compared to dental resin-based materials. Materials 2015; 8: 4751-4767.
22. Wang ZZ, Gu P, Zhang Z. Indentation and scratch behavior of nano-SiO2/polycarbonate composite coating at the micro/nano-scale. Wear 2010; 269: 21-25.
23. Kim MJ, Choi MU, Kim CW. Activation of phospholipase D1 by surface roughness of titanium in MG63 osteoblast-like cell. Biomaterials 2006; 27: 5502-5511.
24. Monemian EA, Rosenbohm J, Reddy K, Jin X, Bouzid T, Riehl B, Kim E, Lim JY, Yang R. Tissue regeneration from mechanical stretching of cell-cell adhesion. Tissue Eng Part C Methods. 2019; 25: 631-640.
25. Zhou M, Smith AM, Das AK, Hodson NW, Collins RF, Ulijn RV, Gough JE. Self-assembled peptide-based hydrogels as scaffolds for anchorage-dependent cells. Biomaterials 2009; 30: 2523-2530.
26. Pranjal N, Cheng Zhang, Victor K. Champagne, Benjamin Boesl, Arvind Agarwal. *In-situ* mechanical investigation of the deformation of splat interfaces in cold-sprayed aluminum alloy. Mater Sci Eng 2018; 737: 297-309.
27. Consiglio R, Randall NX, Bellaton B, von Stebut J. The Nano-scratch Tester (NST) as a new tool for assessing the strength of ultrathin coatings and the mar resistance of polymer films. Thin Solid Films 1998; 332:151-156.
28. Bull SJ. Can the scratch test ever be quantitative Adhesion measurement of films and coatings. Zeist 2001; 2: 107.
29. Legerstee K, Houtsmuller AB. A layered view on focal adhesions. Biology 2021; 10: 1189.
30. Horton ER, Byron A, Askari JA, Ng DH, Millon-Frémillon A, Robertson J, Koper EJ, Paul NR, Warwood S, Knight D, Humphries JD. Definition of a consensus integrin adhesive and its dynamics during adhesion complex assembly and disassembly. Nat Cell Biol 2015; 17: 1577–1587.
31. Bachmann M, Kukkurainen S, Hytönen VP, Wehrle-Haller B. Cell adhesion by integrins. Physiol Rev 2019; 99: 1655-1699.
32. Geiger B, Yamada KM. Molecular architecture and function of matrix adhesions. Cold Spring Harb Perspect Biol 2011; 3: a005033.
33. Pasapera AM, Schneider IC, Rericha E, Schlaepfer DD, Waterman CM. Myosin II activity regulates vinculin recruitment to focal adhesions through FAK-mediated paxillin phosphorylation. J Cell Biol 2010; 188: 877-890.
34. Carisey A, Tsang R, Greiner AM, Nijenhuis N, Heath N, Nazgiewicz A, Kemkemer R, Derby B, Spatz J, Ballestrem C. Vinculin regulates the recruitment and release of core focal adhesion proteins in a force-dependent manner. Curr Biol 2013; 23: 271–281.
35. Zacharchenko T, Qian X, Goult BT, Jethwa D, Almeida TB, Ballestrem C, Critchley DR, Lowy DR, Barsukov IL. LD motif recognition by talin: Structure of the talin-DLC1 complex. Structure 2016; 24:1130-1141.
36. Deakin NO, Ballestrem C, Turner CE. Paxillin and Hic-5 interaction with vinculin is differentially regulated by Rac1 and RhoA. PLoS One 2012; 7: e37990.
37. Li H, Guo C, Zhou Y, Sun H, Hong R, Hamilton DW. Titanium substratum roughness as a determinant of human gingival fibroblast fibronectin and α-smooth muscle actin expression. Materials 2021; 14: 6447.
38. Jung RE, Holderegger C, Sailer I, Khraisat A, Suter A, Hämmerle C. The effect of all-ceramic and porcelainfused-to-metal restorations on marginal peri-implant soft tissue color: A randomized controlled clinical trial. Int J Periodontics Restorative Dent 2008; 28: 357-365.
39. de Moura Costa PV, Serra Ferreira M, Veríssimo C, Miranda de Torres É, Valladares-Neto J, Garcia Silva MA. Is zirconia better than titanium abutments for soft tissue color: A systematic review and meta-analysis of spectrophotometric evaluation. Int J Oral Maxillofac Implants 2021; 36: 875-884a.

***Correspondence to:**

Kazuyoshi Baba

Department of Prosthodontics

School of Dentistry

Showa University

Kitasenzoku, Oota-ku

Tokyo 145-8515

Japan